Article

# Nitrate Mediated Alcohol Oxidation on Cadmium Sulfide Photocatalysts

John DiMeglio, Andrew G Breuhaus-Alvarez, Siqi Li, and Bart M Bartlett

*ACS Catal.*, **Just Accepted Manuscript** • DOI: 10.1021/acscatal.9b01051 • Publication Date (Web): 08 May 2019

# Nitrate Mediated Alcohol Oxidation on Cadmium Sulfide Photocatalysts

John L. DiMeglio, Andrew G. Breuhaus-Alvarez, Siqi Li, and Bart M. Bartlett*

Department of Chemistry, University of Michigan, 930 North University Avenue, Ann Arbor, Michigan 48109, United States

*KEYWORDS: Semiconductor photocatalysis, alcohol oxidation, redox mediator, cadmium sulfide, nitrate radical*

**ABSTRACT:** Developing photocatalysts capable of organic oxidations enables the generation of value added products from biomass feedstocks through visible light irradiation. Through a series of non-aqueous photocatalytic experiments, we have uncovered that CdS nanowires catalyze benzyl alcohol (BnOH) oxidation and 5-hydroxymethylfufural (HMF) oxidation. The rate can be improved by introducing nitrate salts that act as a redox mediator in solution. Specifically, nitrate salts of lithium, magnesium, calcium, and manganese promote the selective photooxidation of BnOH to benzaldehyde on CdS in 70–100 % yields at rates up to 13.6 mM•h$^{-1}$, compared to 8 % yield at 3 mM•h$^{-1}$ in the absence of a nitrate mediator. Kinetic analysis reveals that in the absence of nitrate salts, the reaction is first order with respect to BnOH, while in the presence of nitrate, the reaction is half order in BnOH. This rate law disparity, along with radical trapping and kinetic isotope experiments suggest that nitrate-mediated alcohol oxidations proceed through a mechanism involving the catalytic generation of a nitrate radical, $NO_3$•. The generation of this radical also enables the selective photooxidation of HMF to 2,5-diformylfuran at a rate of 2.6 mM•h$^{-1}$ using CdS nanowires.

## INTRODUCTION

Biomass upgrading represents a unique opportunity for the renewable generation of valuable chemicals and fuels from abundant cellulosic waster mater.[1] Feedstocks for these processes include residues separated from the processing of agricultural products such as rice or sugarcane, which total over 300 megatonnes•y$^{-1}$.[2] While some of this matter is burned as fuel in processing facilities, this is a low-value use of biomass waste. In particular, these lignocellulose materials contain a variety of aromatic species as well as nitrogen and oxygen functional groups that can be used for the generation of value-added platform chemicals.[3] One pathway to isolate a chemical precursor from cellulose involves a series of hydrolysis and dehydration reactions to yield 5-hydroxymethylfurfural (HMF).[4] As shown in **Figure 1**, HMF contains significant chemical

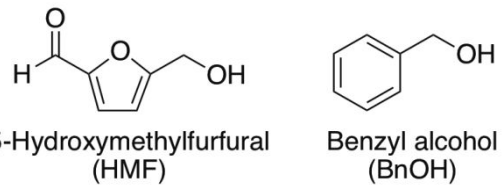


**Figure 1.** Structure of the bio-derived HMF (left) and the model substrate used in this study, BnOH (right).

complexity owing to its aldehyde, alcohol, and furan functionalities. Through these functional groups, HMF can be oxidized to a variety of species, including the polymeric precursors: 2,5-diformylfuran and 2,5-furandicarboxylic acid.[5]

Given the high value of oxidized HMF products, significant efforts have been directed at preparing efficient and selective organic oxidation catalysts.[6,7] Historically, some of the best catalysts include enzyme-based biocatalysts,[8] homogeneous manganese and cobalt salts,[9] as well as carbon or aluminum supported Au, Pt, Pd, and Ru thermal catalysts.[6,7,10] While these catalyst systems display high yield and selectivity for oxidized HMF products, many require high oxygen pressure, temperature, or the addition of a precious metal co-catalyst. In addition to traditional thermal catalysis, photo(electro)catalysts composed of metal oxides or sulfides can also deliver oxidized organic products.[11–13] Photocatalysis enables oxidative chemistry under ambient conditions while using renewable solar energy inputs. However, compared to the wealth of reports on thermal HMF oxidations, there are fewer examples of HMF photo(electro)chemical oxidations. Instead, most reports apply benzyl alcohol (Figure 1, BnOH) as a model compound for the alcohol functionality in HMF.[14–20]The fastest alcohol oxidation rates occur on CdS/graphite/$TiO_2$ ternary platforms and cyanamide functionalized graphitic carbon nitride materials interfaced with molecular electrocatalysis such as cobalt thioporphyrazine or nickel bis(diphosphine) catalysis.[14,21,22]

While interfacing electrocatalysts can significantly improve the efficiency and activity of organic photooxidations, this approach is limited by the cost and preparation of the co-catalyst or the synthetic complexity of

a multi-component material. As an alternative to surface catalyst incorporation, many electrochemical,[23–25] photochemical[26–28] and photoelectrochemical organic oxidation reactions rely on *N*-oxyl radical mediators such as 2,2,6,6,-tetramethylpiperidinyloxyl (TEMPO) to improve their catalytic activity. Mediators like TEMPO function by undergoing facile oxidation at a particle or electrode surface followed by homogeneous charge transfer with the substrate. This homogeneous charge transfer has unique reactivity compared to direct heterogenous charge transfer, enabling the oxidation of various inactivated compounds.[29,30] In particular, reactions employing $TiO_2$, ZnO and $Fe_2O_3$ have demonstrated significant alcohol oxidation rate increases in the presence of *N*-oxyl mediators.[26–28] Alternatively, Ni-modified CdSe quantum dots may also mediate alcohol oxidations through their thiol-based capping ligands.[31] While the catalytic properties of *N*-oxyl mediators have been well established, there are a variety of redox mediators including simple organic compounds and commercially available salts that have not yet been fully investigated.[32–34]

One particularly promising mediator class that may have applications in photocatalysis are nitrate salts. Previous electrochemical work has demonstrated nitrate-mediated alcohol oxidations on carbon and platinum electrodes.[35–37] In addition to electrochemical mediation, the nitrate ion/nitrate radical couple ($NO_3^-/NO_3\bullet$) is involved in atmospheric volatile organic compound oxidations.[38,39] This reactivity towards organic compounds has also been applied to solution oxidations, where nitrate radical generation occurs by laser flash photolysis or radiolysis of dissolved nitrate salts.[40–42] In addition to these generation methods, photochemical nitrate radical formation is possible by $TiO_2$ in aqueous nitrate solutions.[43] Despite these promising characteristics, alcohol oxidation mediated by nitrate has been limited to gas phase $TiO_2$ applications[44] and homogenous oxidations on organic dyes.[45] However, these acridinium-based light absorbers are challenged by their inherent reactivity towards nitrate radicals.

To test the ability of nitrate-based mediators to promote primary alcohol oxidation reactions, we first employed BnOH as a bio feedstock model substrate.[46] CdS nanowires act as the photocatalyst, and have the advantages to its excellent photophysical properties and established reactivity with organic substrates.[47–49] We carried out reactions in acetonitrile to minimize aqueous hydroxy radical formation and to maximize substrate solubility.[50] Herein, we show that unfunctionalized CdS nanowires are capable of yielding benzaldehyde at maximum rate of 13.6 $mM\bullet h^{-1}$ from 2 mL solutions containing 0.1 mmol of $Mn(NO_3)_2$ and 1 mg CdS illuminated with 170 W 465 nm blue LED light. Moreover, we validate using BnOH as a model by also demonstrating that HMF is selectively oxidized to 2,5-diformylfuran (DFF) under the same conditions at a rate of 2.6 $mM\bullet h^{-1}$.

## RESULTS

To test the catalytic activity of nitrate-based redox mediators for organic oxidations on semiconductors, we performed BnOH photocatalysis as shown in **Equation 1**.

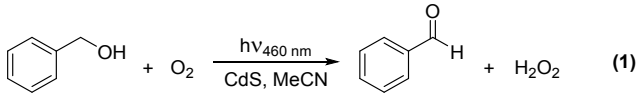

(1)

After two days of irradiation in a BnOH solution without any mediator, the CdS nanowires produced a trace quantity of benzaldehyde in 7 ± 0.5 % yield. Upon adding 50 mM lithium nitrate, the benzaldehyde yield increased by an order of magnitude to 70 ± 10 %. Kinetic analysis performed during the first eight hours of the reaction show that initial rate for benzaldehyde production increases from 3 to 10 $mM\bullet h^{-1}$ when lithium nitrate is added. Gas chromatography reveals that benzaldehyde is the only product detected, giving rise to >99 % selectivity (Figure S1). Control reactions performed without CdS, in the dark, or under nitrogen display significantly suppressed benzaldehyde yields, highlighting that this is a photocatalytic process that requires CdS, lithium nitrate, oxygen, and light (Figure S2).

To elucidate further the importance of nitrate in the reaction, we conducted a control experiment with $LiPF_6$ (nitrate-free). After two days of photocatalysis using this alternate $Li^+$ salt, the benzaldehyde yield drops to 18 ± 7 %, demonstrating that $NO_3^-$ is critical to the observed catalysis. Based on these control experiments and established nitrate radical chemistry (vide supra), we hypothesize that CdS oxidizes $NO_3^-$ to the $NO_3\bullet$ nitrate radical, which then mediates BnOH oxidation to benzaldehyde.

While the low photocatalytic BnOH activity of $LiPF_6$ solutions supports that nitrate is required for the observed catalysis, we next sought to determine if $Li^+$ is required for the observed reactivity. The nitrate salts of calcium, magnesium, and manganese are at least partially soluble in acetonitrile solvent at 50 mM. **Figure 2** (red bars) shows

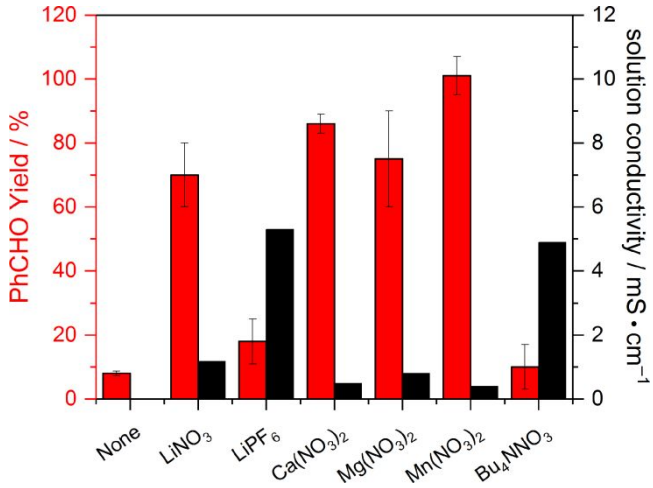


**Figure 2.** Average benzaldehyde yield (red) from a two day irradiation of CdS suspensions in acetonitrile with the listed meditator at 50 mM, and the electrical conductivity of the solution (black). Error bars represent the standard deviation among 3 trials.

that all of these metal cations catalyze BnOH oxidation to benzaldehyde in 70-100 % yield. However, the tetrabutylammonium cation ($Bu_4N^+$) displays a much lower yield, only 10 ± 7 %, nearly that that of the unmediated reaction. The low $Bu_4NNO_3$ reactivity may be rationalized by measuring solution conductivity, which directly relates

to ion activity. Solution conductivity measurements reveal that lithium, calcium, magnesium and manganese nitrate show conductivity values ≤ 1.2 mS/cm, while both the $Bu_4NNO_3$ and $LiPF_6$ solutions display conductivities of ~5 mS/cm (**Figure 2**, black bars).

In addition to conductivity measurements, solution FT-IR analysis in **Figure 3** shows an ~10 $cm^{-1}$ bathochromic

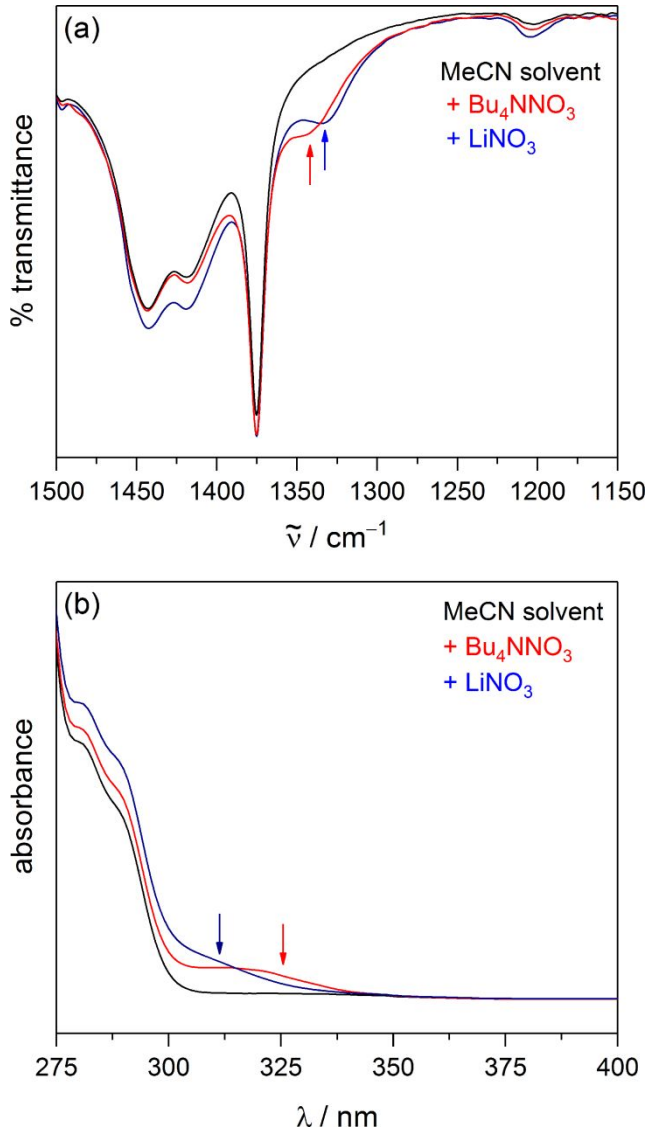


**Figure 3.** FTIR (a) and UV-Vis (b) spectra of $LiNO_3$ and $Bu_4NNO_3$ in MeCN.

shift of the $LiNO_3$ N-O frequency compared to that of $Bu_4NNO_3$. Furthermore, UV-Vis spectra acquired of the same solutions (Figure 3b) display a hypsochromic shift in the electronic absorption, as has been previously demonstrated with $Ca(NO_3)_2$.[51]

**Figure 4** shows that individually, $LiPF_6$ and $Bu_4NNO_3$ are inert toward photocatalytic BnOH oxidation (black and red profiles, respectively). However the photocatalytic reaction of a solution containing both $LiPF_6$ and $Bu_4NNO_3$ yields a catalytic profile closely resembling that observed for $LiNO_3$ (blue and green profiles, respectively). This experiment is repeated in Figure S3. This recovery of catalysis supports that metathesis in solution generates the active $LiNO_3$ species, enabling BnOH oxidation. Moreover, having either $Bu_4N^+$ or $PF_6^-$ in solution does not inhibit the reaction.

To probe the nature of nitrate-enhanced BnOH oxidation further, we analyzed the initial rate during the first eight

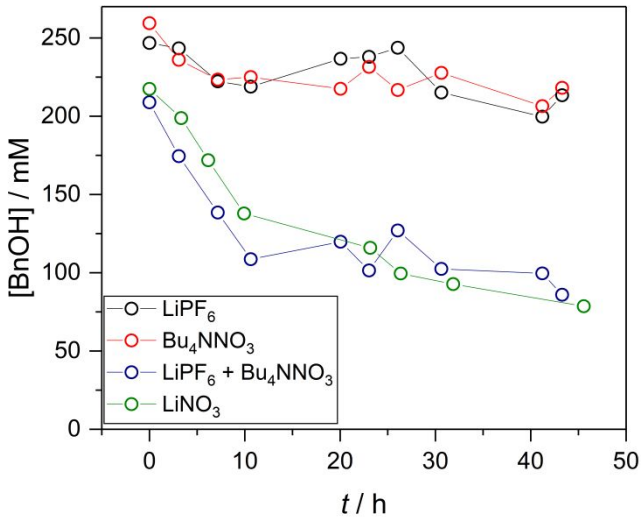


**Figure 4.** Concentration of BnOH over time, upon CdS photocatalysis of $LiPF_6$ (black), $Bu_4NNO_3$ (red), $LiPF_6$ (green), or a $Bu_4NNO_3$ and $LiPF_6$ mixture (blue) in acetonitrile solutions.

hours of the reaction using gas chromatography to quantify BnOH consumption (Figure S4). **Figure 5**a shows that

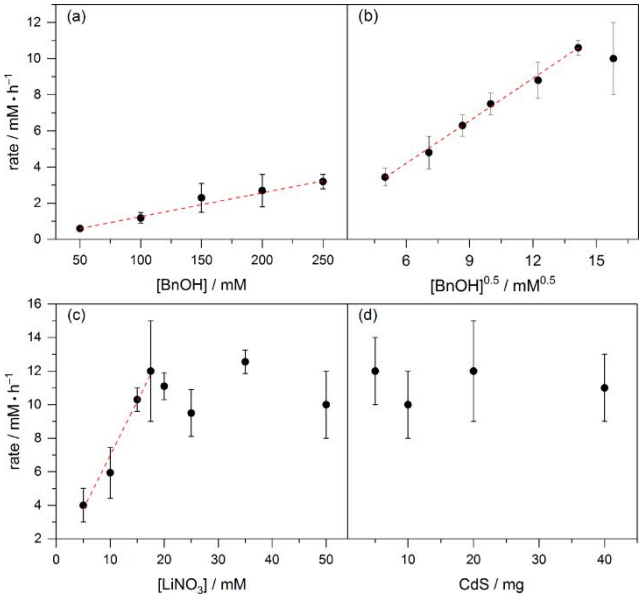


**Figure 5.** Kinetic plots for illumined CdS samples in solutions with various BnOH concentrations for mediator-free (a) and $LiNO_3$ containing solutions (b); as well as solutions with varying $LiNO_3$ (c) or CdS loading (d). The highest concentration were omitted from analysis due to surface site saturation.

without any mediator, the reaction is first order in BnOH However, with $LiNO_3$ in solution, the reaction is *half order* in BnOH (Figure 5b). In addition, the reaction is first order in $LiNO_3$ (Figure 5c) and zero order in CdS near our 10 mg loading (Figure 5d). The zero-order photocatalyst dependence likely arises because of light scattering (Figure

S5). In accord with the half-order dependence on [BnOH], the slope of the plot of $[BnOH]^{1/2}$ vs. *t* starting from 250 mM BnOH is linear over the first 10 h of the reaction and provides an initial rate constant ~ 0.6 $mM^{1/2}\,h^{-1}$ (Figure S6).

While the catalytic behavior we observe with CdS and $NO_3^-$ is indicative of $NO_3$• formation, we do not directly observe any adsorbed nitrate species by *ex-situ* Raman spectroscopy (Figure S7), infrared spectroscopy (Figure S8), X-ray photoelectron spectroscopy (Figure S9), or *in situ* electron paramagnetic resonance spectroscopy (Figure S10). We surmise that any $NO_3$• that is formed is very reactive, and therefore short lived. While Raman analysis displays no adsorbed nitrate signals, a small change in the Raman overtone intensity, attributed to CdS surface trap state formation was observed.[52] We propose that these trap states are a result of CdS corrosion, which has been previously observed during non-aqueous CdS photocatalysis.[53] Emerging infrared stretching frequencies are also consistent with the formation of a sulfate species (Figure S8). Ultimately, scanning electron microscopy imaging shows a significant morphological change in the CdS nanowires after the photocatalytic reaction with BnOH (Figure S11), corroborating their corrosion. In addition to this loss of morphology, inductively coupled plasma mass spectrometry carried out on solution after the reaction detects leached cadmium at 106 ± 5 ppm. X-ray photoelectron spectroscopy (XPS) also confirms surface corrosion by the appearance of 48 ± 2 % sulfate (Figure S12). Further XPS experiments reveal detectable lithium on the particle surface in the form of lithium sulfate, which would result from $Li^+$ transmetalation of $Cd^{2+}$. The presence of crystalline lithium sulfate was further confirmed through powder X-ray diffraction (PXRD) on the CdS nanowire photocatalysts after the reaction (Figure S13).

Therefore, in order to further ascertain the function of nitrate in this system, we performed photocatalytic BnOH oxidation in the presence of a nitrate radical trap, tetramethylethylene (TME).[54,55] **Equation 2** shows one reaction

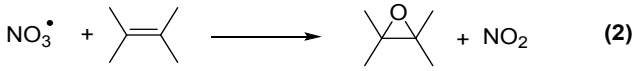


(2)

between $NO_3$• and TME, olefin epoxidation that liberates $NO_2$. **Figure 6** shows that when TME is added to a nitrate-free BnOH solution, the photocatalytic reaction rate is unaffected (blue trace vs black trace; Figure S14). However, when TME is introduced into $LiNO_3$ containing solution, the catalytic activity significantly decreases (red vs. green traces), and the reactivity reverts to that of unmediated reaction (black trace).

To elucidate the key steps in which this nitrate radical facilitates BnOH conversion, we investigated the kinetic behavior of a deuterated BnOH substrate. Upon CdS photocatalysis of a $LiNO_3$ solution containing benzyl alcohol-α,α-$d_2$, **Figure 7** shows a negligible kinetic isotope effect (KIE) of 1.2 ± 0.3 for deuterated benzaldehyde production (Figure S15), indicating that α-deprotonation is not rate-determining. Additionally, CdS BnOH photocatalysis performed in the presence of $^{18}O_2$ yields benzaldehyde with no $^{18}O$ incorporation, suggesting that oxygen atom transfer from reduced oxygen species does not occur in this system (Figure S16), in contrast to $TiO_2$ BnOH photocatalysis.[12]

Nitrate-mediated CdS photocatalysis also oxidizes HMF, a true bio-derived substrate, as illustrated in **equation 3**.

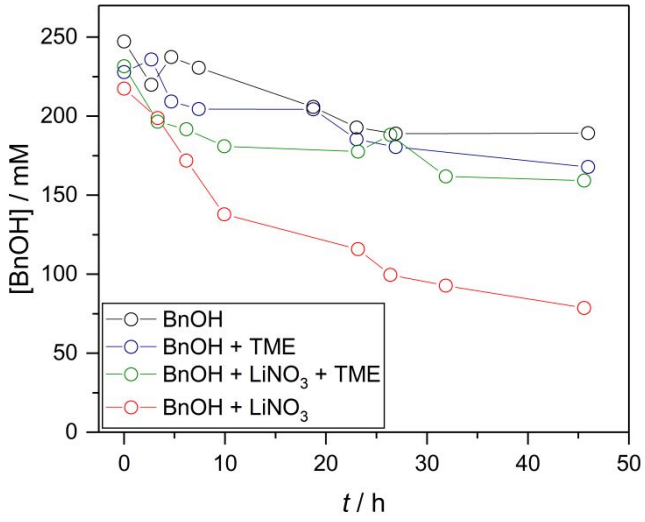


**Figure 6** Concentration of BnOH over time, upon photocatalysis of a mediator free solution (black), a mediator free solution with TME (blue), a $LiNO_3$ solution with TME (green), and a $LiNO_3$ solution (red).

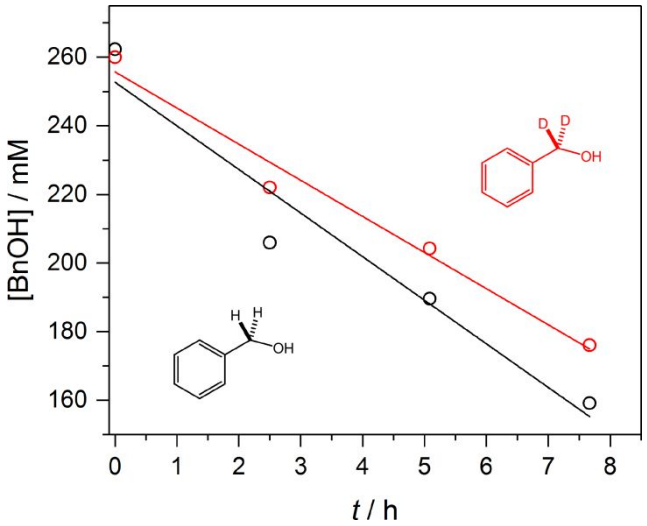


**Figure 7.** Concentration of BnOH over time during CdS photocatalysis with $LiNO_3$ in acetonitrile when using protonated (black) and deuterated (α,α-$d_2$) benzyl alcohol (red).

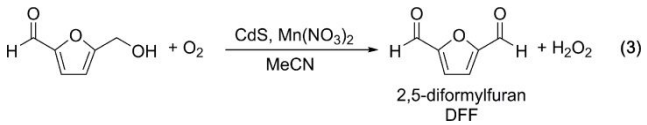


(3)

**Figure 8** shows that in the presence of $Mn(NO_3)_2$, quantitative conversion to 2,5-diformyl-furnan (DFF) occurs between 24 and 48 h with an initial rate of 2.6 mM•$h^{-1}$. When the nitrate mediator was removed from the solution, *no* HMF oxidation was observed (Figure S17).

## DISCUSSION

Expanding selective catalysts for organic oxidations to include heterogeneous photocatalysts is challenging because of the low activity of unfunctionalized light absorbers. Consequently, most preliminary photocatalytic transfor-

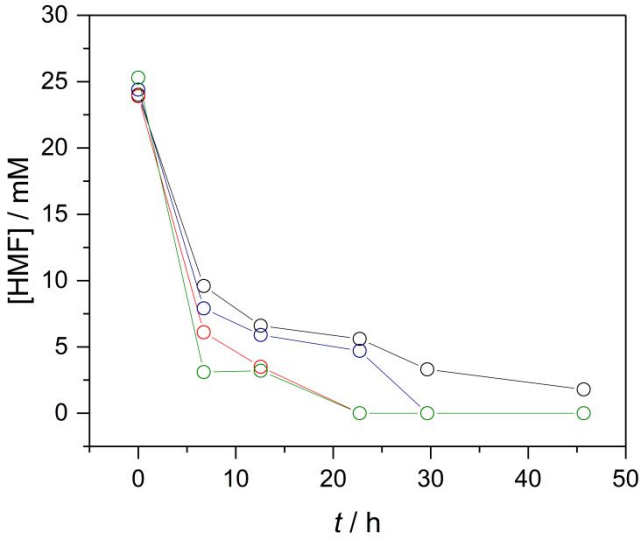


**Figure 8.** Concentration of HMF over time using $Mn(NO)_3$ as a mediator. Data for four separate trials are presented.

mations target amine-based substrates due to their electron-rich functionality, which leads to facile oxidation.[56] Materials such as $BiVO_4$,[57] $CuWO_4$,[11] $TiO_2$[58] and CdS[47–49,53] establish that semiconducting photocatalysts can selectively deliver imines from amines. While amines serve as an excellent test reaction for evaluating photocatalysts, alcohols are a far more lucrative substrate since they are bioavailable from agricultural feedstocks, and their oxidized products have value.[59] In particular, significant efforts are aimed at cellulose-derived HMF oxidation to yield products including 2,5-furandicarboxylic acid and 2,5-diformylfuran (DFF), as valuable precursors for furan-based polyesters[60] and furanic poly Schiff bases.[61]

**Table 1** compares the BnOH and HMF activity of our nitrate mediated CdS platform with representative examples of other heterogeneous photocatalysts. These materials highlight the various classifications of heterogenous photocatalytic materials active for alcohol oxidation, including: unfunctionalized metal oxides, multijunction catalysts, photocatalysts modified with precious metal or homogeneous catalysts, and reactions performed with redox mediators. In these studies, BnOH is a biomass model compound and displays high selectivity for aldehyde formation over carboxylic acid products. While catalyst and substrate loading are not standardized, the reaction rate typically increases with the use of complex photocatalyst design or with metal co-catalysts. Generally, the highest reported rates for alcohol oxidation are observed with multi-junction CdS,[62–64]cyanamide functionalized graphitic carbon nitride materials interfaced with molecular electrocatalysis such as cobalt thioporphyrazine or nickel bis(diphosphine) catalysis,[22,65] and dye-sensitized ZnO photochemistry performed in the presence of the *N*-oxyl redox mediator, TEMPO.

Compared to these previously reported examples, we find that our optimized conditions comprising 2 mL acetonitrile containing 50 mM $Mn(NO_3)_2$ with 1 mg of suspended CdS nanowires with 250 mM BnOH substrate yields benzaldehyde exclusively with an initial rate of 13.6 $mM \cdot h^{-1}$, which is competitive with some of the most active systems

**Table 1.** Comparison of various heterogeneous alcohol oxidation photocatalysis. Rates were calculated from the kinetic data presented in the listed references

| Photocatalyst | Solvent | Substrate | Product | Selectivity / % | Rate / $mM \cdot h^{-1}$ |
|---|---|---|---|---|---|
| **$TiO_2$**[15] | Water | Me-BnOH | Me-BnAl | 60 | 0.21 |
| **$HNb_3O_8$**[17] | BTF | BnOH | BnAl | >99 | 3.3 |
| **P-$Zn_xCd_{1-x}S$**[14] | Water | HMF | DFF | 65 | 0.16 |
| **$In_2S_{3-x}$**[20] | BTF | BnOH | BnAl | >99 | 7.1 |
| **CdS/Graphite/$TiO_2$**[62] | BTF | BnOH | BnAl | 90 | 16 |
| **$WO_3/TiO_2$**[64] | Water | BnOH | BnAl | 56 | 2 |
| **Ni/CdS**[63] | Water | FFA | Furfural | >99 | 2 |
| **$Au/CeO_2$**[16] | Water | BnOH | BnAl | >99 | 0.8 |
| **CoPz, g-$C_3N_4$**[22] | Water | HMF | FDCA | 97 | 1.6 |
| **Ni-P, g-$C_3N_4$**[19] | Water | MeO-BnOH | MeO-BnAl | >99 | 6.6 |
| **Ni / MPA-CdSe**[31] | Water | BnOH | BnAl | 98 | 3 |
| **DS-ZnO**[27] | Water / TEMPO / $Ag^+$ | BnOH | BnAl | >99 | 27 |
| **DS-$TiO_2$**[26] | BTF / TEMPO | BnOH | BnAl | 98 | 4 |
| **CdS** | MeCN / $Mn(NO_3)_2$ | BnOH | BnAl | >99 | 13.6 |
| **CdS** | MeCN / $Mn(NO_3)_2$ | HMF | DFF | >99 | 2.6 |

Abbreviations: BnOH = Benzyl Alcohol, BnAl = Benzaldehyde, HMF= 5-hydroxymethylfurfural, DFF = 2,5-diformylfuran, FFA = furfuryl alcohol, MeO-BnOH = 4-methoxy benzyl alcohol, MeO-BnAl = 4-methoxybenzaldehyde, Me-BnOH = 4-methyl benzyl alcohol, Me-BnAl = 4-methyl benzaldehyde, BTF = trifluorotoluene, MeCN = acetonitrile, CoPz = cobalt thioporphyrazine, Ni-P = nickel bis(diphosphine) DuBois catalyst, MPA-CdSe = mercaptopropionic acid-capped CdSe quantum dots, DS-ZnO and DS-$TiO_2$ = dye sensitized ZnO and $TiO_2$, respectively.

reported to date, *without the use of metal co-catalysts or multi-phase photocatalysts*. We note that optimization involves improving the photocatalyst dispersion using a 10-minute sonication (Figure S18), an enhancement that has been previously reported for carbon nitride.[21] While the rate of BnOH oxidation in this system is very competitive, corrosion of the CdS material as shown through SEM imaging, XPS-, PXRD-, and ICP-MS analysis (vide supra) limits the recyclability of the photocatalyst material. The photocatalytic activity of the CdS nanowires continuously drops over the five days that it shows activity (Figure S19).

While nitrate salts of $Li^+$, $Mg^{2+}$, $Ca^{2+}$, and $Mn^{2+}$ catalyze alcohol oxidation, $Bu_4NNO_3$ has no effect on the reaction rate (Figure 2). We rationalize this reactivity by considering the solution conductivity and hard soft acid- base concepts. In acetonitrile, hard metal ions tend to bind tightly to the hard nitrate ion, leading to generally low solubility. The soft $Bu_4N^+$ cation and soft $PF_6^-$ anion lead to high solubility for $Bu_4NNO_3$ and $LiPF_6$. We find that catalysis results only from the partially associated ionic solids. Moreover, *in situ* formation of $LiNO_3$ from the metathesis of the soluble salts $Bu_4NNO_3$ and $LiPF_6$ gives rise to nearly the same reactivity and suppressed conductivity (Table S1) observed in the pristine $LiNO_3$ solution. That is, the other cations do not inhibit substrate binding or subsequent oxidation.

FT-IR and UV-Vis spectroscopy of $Li^+$ and $Bu_4N^+$ acetonitrile solutions corroborated an associated metal cation-nitrate interaction. Figure 3a shows a bathochromic shift in the N-O stretching vibration in $LiNO_3$ compared to $Bu_4NNO_3$ , suggesting a stronger interaction between $Li^+$ and $NO_3^-$ in acetonitrile. Similar IR spectra shifts have been reported for the effect of water coordination on differently hydrated nitrate ions, $NO_3^-(H_2O)_{1\text{-}6}$ .[66] In addition to FT-IR evidence of a strong Li-$NO_3$ interaction, we find that $Li^+$ cations also result in a hypsochromic shift the $NO_3^-$ UV-Vis absorption profile as shown in Figure 3b. Previous UV-Vis spectra reported for $Ca(NO_3)_2$ shows that a stronger cation-nitrate interaction blue shifts the absorption due to the reduced symmetry and conjugation of a metal-nitrate species compared to free or more weakly coordinated ntirate.[51] The exact nature of this interaction and its importance to the photocatalytic oxidation of BnOH on CdS is unclear. We hypothesize that the relatively stronger metal-nitrate interaction (compared to $Bu_4NNO_3$) may facilitate nitrate radical desorption from CdS required to mediate homogeneous electron transfer.

The reaction order with respect to BnOH substrate differs whether or not metal nitrates are present, suggesting that the reactions proceed by different mechanisms. Without the $NO_3^-$ mediator, the reaction is first-order in BnOH, but with $LiNO_3$ present, we observe a half-order dependence in BnOH (Figure 5). Without nitrate, the CdS activity is likely limited by heterogeneous charge transfer to BnOH as is commonly proposed in photocatalytic reactions.[67] We propose that the half-order dependence with nitrate arises as $NO_3$• radical oxidizes benzyl alcohol. This reaction order and proposed mechanism are similar to what is proposed for electrochemical BnOH oxidation mediated by (bpy)Cu/TEMPO,[23] where the catalytic current is half order in BnOH substrate. These results agree with established electrokinetic models of homogeneous systems limited by chemical steps involving the catalyst.[68] and also match what has been observed experimentally with adsorbed $CrO_4^-$ reduction on $TiO_2$.[69]

The fractional reaction order suggests that BnOH oxidation on our $LiNO_3$/CdS system proceeds through a different mechanism than on CdS, we next sought to obtain evidence for the proposed nitrate radical intermediate. Previous reports indicate that TME is highly sensitive to the presence of nitrate radical and will quickly undergo oxidation to a variety of oxygenated products, including epoxides as shown in equation 2.[54,55] The kinetic experiments in Figure 6 reveal that TME inhibits the photocatalytic activity of nitrate-containing solutions, suggesting that any generated nitrate radical preferentially reacts with TME over BnOH. Importantly, TME has no effect on the native, nitrate-free CdS BnOH activity, highlighting that TME does not compete with BnOH for surface sites. Based on the established reactivity of alkenes as traps for nitrate radical and the suppression of nitrate catalysis in the presence of TME, we propose that catalytic nitrate oxidation to nitrate radical is an elementary step in catalytic 1° alcohol oxidation.

In addition to nitrate oxidation to nitrate radical, there are a diverse set of electrochemical pathways in which nitrate may serve as an oxidizing agent through the formation of either nitrous oxide, nitric acid, or nitrogen dioxide (Figure S20). While stoichiometric consumption of nitrate is unlikely as catalysis yields benzaldehyde concentrations higher than the lithium nitrate concentration, we sought to quantify nitrate consumption through gravimetric analysis. An excess of sodium perchlorate was added to a series of solutions isolated after photocatalysis, yielding a white precipitate shown to be sodium nitrate by PXRD analysis (Figure S21). Based on the isolated solid, we calculated a nitrate recovery of 90 ± 10 %, supporting that nitrate is not consumed in this reaction. While gravimetric analysis supports the catalytic nature of nitrate under aerobic conditions, we found a significant drop in solution nitrate concentration in those reactions carried out under $N_2$. This nitrate consumption suggests that the small PhCHO yields detected under $N_2$ are due to BnOH oxidation coupled with *stoichiometric* nitrate oxidation. Investigations into the nature of anaerobic BnOH mediation is a subject of ongoing study in our laboratory. From the kinetic experiments outlined above, we propose the mechanism shown in **Error! Reference source not found.**. Principally,

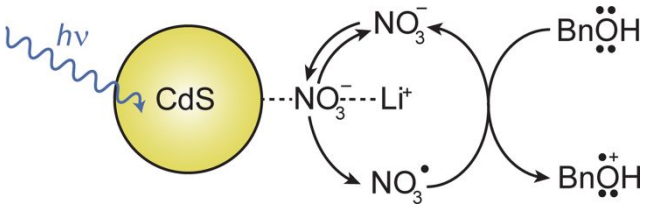


**Scheme 1.** Proposed mechanism for $LiNO_3$ mediated photocatalytic oxidation of benzyl alcohol.

photocatalytic oxidation of nitrate to a nitrate radical species occurs. Cations such a lithium participate either in nitrate absorption/desorption or intermediate stabilization. In accordance with previous mediated mechanisms we suggest that the nitrate radical desorbs from the surface and interacts with BnOH in a rate determining electron transfer process.[32–34] The nitrate radical intermediate likely reacts with BnOH in an electrochemical process without coupled α-proton abstraction, as no significant KIE (1.2 ± 0.3) was observed (Figure 7). Further studies are required to elucidate the mechanistic steps following nitrate-meditated substrate oxidation. However, given that isotopically labeled $^{18}O_2$ does not support oxygen-atom transfer from reduced oxygen in this reaction (Figure S16), it is unlikely that previously proposed mechanisms for non-aqueous $TiO_2$ photocatalysis are operative. [12, 70] We surmise that superoxide radical generated from photogenerated electrons serves as a base and another nitrate radical mediates the second electron transfer necessary for benzaldehyde formation.

Through these studies we have established that nitrate salts dissolved in acetonitrile are capable of mediating BnOH oxidation. To test the ability of other common mediators for CdS promoted BnOH oxidation we performed photocatalysis in solutions containing triarylamines, polycyclic aromatic hydrocarbons, perchlorate and halide salts (Figure S22).[32–34] After two days of illumination, we found that of the tested mediators, only lithium salts of bromine and chlorine displayed improved benzaldehyde conversions of 60 ± 10 % and 62 ± 9 %, respectively. While these halide mediators promote BnOH oxidation, PXRD carried out after the reaction revealed significant CdS corrosion in lithium halide solutions compared to nitrate (Figure S13).

## CONCLUSIONS

Photocatalytic BnOH oxidation on CdS particles is significantly enhanced in the presence of either lithium, magnesium, manganese, or calcium nitrate salts. These reactions yield benzaldehyde selectivity at a rate of 13.6 $mM \bullet h^{-1}$. Through a series of kinetic and trapping experiments we propose that benzaldehyde is produced through a mechanism involving the formation of a nitrate radical which oxidizes the alcohol substrate rather than direct oxidation by photogenerated holes. In addition to promoting BnOH oxidation, this nitrate radical mediator can direct the course of HMF oxidation to selectively deliver 2,5-diformylfuran at a rate of 2.6 $mM \bullet h^{-1}$. Through the course of this study, we have determined that tetrabutylammonium cations are not compatible with nitrate-based catalysis, likely due to a weaker nitrate interaction. These results present the application of simple nitrate salts to mediate oxidations relevant to biomass upgrading, and present new opportunities and challenges for continued studies of mediated photocatalytic systems.

## EXPERIMENTAL

**Materials and Methods.** All solvents were purchased from Sigma Aldrich and used without further purification. All alcohols were purchased from Fisher scientific, the mediator salts and deuterated benzyl alcohol were purchased from Sigma Aldrich. Nylon Syringe filters (25 mm, 0.2 mm membrane) were purchased from VWR. To achieve 50 mM $LiNO_3$ concentrations mixtures of $LiNO_3$, MeCN and BnOH were prepared and then sonicated under heat (~50 ℃) for 20 minutes to give a clear, colorless solution.

**Preparation of CdS Nanowires.** CdS Nanowires (NWs) were prepared by adopting a previously reported hydrothermal synthesis.[71] Cadmium nitrate tetrahydrate (751 mg, 2.4 mmol), thiourea (556 mg, 7.3 mol), and ethylenediamine (13 mL) were mixed in an 18 mL PTFE lined autoclave. The vessel was sealed and warmed to 160 ˚C at a of 10 ˚C/min ramp rate. After two days at 160 ˚C the reaction vessel was cooled naturally to room temperature to give a yellow powder suspended in an orange solution. This suspension was centrifuged at 4000 rpm for 5 minutes to isolate a bright yellow powder. This powder was washed four times with Millipore (MQ) water (4 × 15 mL), and then dried overnight in a vacuum oven at 50 ˚C.

**Characterization Details.** Scanning electron microscopy (SEM) images were obtained from a Zeiss LEO 1455VP tungsten filament SEM at an accelerating voltage of 3 kV and working distance of 5 mm. Powder X-ray diffraction (PXRD) data was collected on a Panalytical Empyrean diffractometer at a power of 1.8 kW (45 kV, 40 mA) with Cu K**α** (**λ** = 1.5418 nm) radiation. The diffractometer was a X'Celerator Scientific, a position-sensitive 1D detector and was equipped with a Bragg-Brentano$^{HD}$ X-ray optic delivering only K**α** radiation. Patterns were collected with a sampling step of 0.017 ° and a scan rate of 6 °/min while spinning at a rate of 0.25 Hz. X-ray photoelectron spectroscopy (XPS) was conducted using a Kratos Axis Ultra X-ray Photoelectron Spectrometer. The X-rays used were monochromatic Al K**α** X-rays (1486.7 eV). All data collected while the analysis chamber pressure was ~ $1 \times 10^{-9}$ torr. The charging effects of the semiconducting substrates were compensated using an electron flood gun. High-resolution spectra were collected at a pass energy of 20 and a step size of 0.1 eV. XPS spectra interpretation was performed using Casa XPS with a Shirley-type baseline to calculate peak areas. Binding energies were calibrated by positioning the adventitious carbon signal at 248.8 eV. Raman spectra were collected on a Renishaw inVia microscope equipped with a 532 nm laser. Fourier transform- infrared spectroscopy was performed on a Thermo-Nicolet IS-50 spectrometer equipped with an ATR accessory. UV-VIS spectra were acquired on a Cary 5000 UV-Vis NIR Spectrophotometer. Conductivity measurements were obtained using a Mettler-Toledo FEPO30 conductivity meter equipped with an InLab 710 probe at room temperature.

**Leached Cadmium Detection.** Cadmium concentration in the post photocatalysis solution was determined via inductively coupled plasma mass spectrometry (ICP-MS) using a Perkin-Elmer Nexion 2000 ICP-MS. The post photocatalysis suspension were filtered through a syringe filter, and rinsed with acetonitrile three times (3 x 1 mL). Volatile organics were then removed by rotary evaporation to yield a viscous oil. This oil was dissolved in Milli-Q water and filtered through a new syringe filter. Samples were referenced to an external bismuth standard (20 ppb) and concentrations of cadmium were determined via a series of standard cadmium solution prepared from a 1000 ppm Cd reference solution (Sigma Aldrich).

**In situ EPR Spectroscopy.** In situ EPR spectroscopy was performed on a Bruker EMX electron spin resonance spectrometer at room temperature. Spectra were recorded both in the dark and after 20 minutes of illumination. The resonator cavity used was a 4102-ST cavity. Illumination was provided by a Newport-Oriel 150 W Xe arc lamp to give a power of ~200 mW $cm^{-2}$ as measured by an optical power meter (Newport 1918-R) equipped with a thermopile detector (Newport 818P-015-19). The microwave frequency was set to 9.822 GHz with a power of 20.51 mW. The data was collected with the receiver set to a modulation amplitude of 1 G and a modulation frequency of 100 kHz. The data was converted to g-factor using the following conversion:

$$g = \frac{(h \times \nu)}{(\mu_B \times B_0)}$$

where h = planks constant, $\upsilon$ = microwave frequency, $\mu_B$ is the Bohr magneton, and $B_0$ is the applied magnetic field strength.

**Photochemistry.** CdS (1-40 mg) was suspended in acetonitrile (2 mL) in a borosilicate 15 x 44mm OD 4 mL vial (Kimble) equipped with a stir bar. Unless otherwise noted, all experiments was performed at 250 mM substrate and 50 mM mediator. The vials were capped with a septum (Chemglass 14/20-14/35) and kept under an oxygen atmosphere using a balloon. Prior to illumination, we found that 10 minutes of sonication significantly improves the dispersion and performance of the photocatalyst material. The reaction mixture was placed in a custom-built aluminum LED photoreactor (Figure S23). This photoreactor is equipped with five royal blue LEDs ($\lambda_{max}$ = 460 nm) with a power rating of 1.03 W (Mouser Electronic, Part: 997-LXML-PR02-A900). These LEDs were reflow soldered onto a SinkPAD star board (Adura LED Solutions, Part: 1903), aligned in series and powered using a 12 W 700mA constant current LED driver (semperlite, Part: APC-12-700). While in use, the photoreactor was cooled using a fan to an average temperature of 29.9 ± 0.5 ˚C. The average light intensity was measured to be 170 ± 10 mW $cm^{-2}$. For experiments performed under $^{18}O_2$, a $LiNO_3$ and BnOH solution in MeCN was prepared and degassed through six cycles of freeze-pump-thaw. This degassed solution was brought into a $N_2$ glovebox where 2 mL was dispensed into a vial loaded with 10 mg CdS. This vial was sealed with a septum, brought out of the glovebox and a balloon containing $^{18}O_2$ (97 atom %, Aldrich) was affixed on top. Substrate and product concentrations were measured using GC-FID by periodically removing an aliquot (10 $\mu$L) from the reaction mixture and combining with a chlorobenzene standard (50 $\mu$L of a 21.6 mM standard) and acetonitrile (940 $\mu$L). Before aliquot collection, the solution mass was measured, and any evaporation was corrected by adding an appropriate amount of acetonitrile. Before returning the samples to the reaction vessel, the oxygen balloon was refilled with fresh oxygen. The samples were analyzed on either a Shimadzu QP-2010 GC/MS or Thermo Fisher Trace 13-10 gas chromatograph equipped with a capillary column and FID detector. During analysis the column oven was warmed from 40 to 290 ℃ at a 10 ℃/min ramp rate. Quantification was enabled by the integration ratio of the analyte and chlorobenzene signals in relation to an obtained calibration curve.

**Gravimetric Nitrate Determination**. Nitrate concentrations were determined by addition of excess sodium perchlorate after the photocatalytic reaction. The CdS photocatalyst as separated from the reaction mixture by centrifuging the reaction mixture at 4000 rpm for 5 minutes. The reaction solution was transferred to a tared vial and the CdS was washed with MeCN (3x 2 mL). These washes were combined and a solution of sodium perchlorate (1 M, 4 mL) was added to produce a white precipitate. This suspension was left overnight in a refrigerator. The white solid was then isolated by centrifuging and washed with MeCN (3 x 2 mL). The resulting powder was dried overnight in a vacuum oven at 50 ˚C and was confirmed to be sodium nitrate by PXRD analysis.

## ASSOCIATED CONTENT

## AUTHOR INFORMATION

### Corresponding Author

* (B.M.B) * E-mail: bartmb@umich.edu

### Author Contributions

The manuscript was written through contributions of all authors. / All authors have given approval to the final version of the manuscript.

### Supporting Information

Additional kinetic data, Raman, FTIR, EPR, XPS, FTIR, mass spectra, solution conductivity measurements, images of CdS dispersion, gravimetric analysis results, and images of a custom-built LED photoreactor. The Supporting Information is available free of charge on the ACS Publications website.

## ACKNOWLEDGMENT

This work was supported by the U.S. Department of Energy, Office of Science, Basic Energy Sciences, Catalysis Science Program, under Award # DE-SC0006587. For the XPS instrument, the authors acknowledge the financial support of the University of Michigan College of Engineering and NSF grant #DMR-0420785 and technical support from the Michigan Center for Materials Characterization. In particular, we thank Drs. Kai Sun, Haiping Sun, and Bobby Kerns for assistance. AGBA thanks the University of Michigan Rackham Graduate School for funding through a Rackham Merit Fellowship.

## ABBREVIATIONS

BnOH, Benzyl alcohol; BnAl, Benzaldehyde, HMF, 5-hydroxymethylfurfural; DFF, 2,5-diformylfuran; TME, tetramethylethylene, FFA = furfuryl alcohol, MeO-BnOH = 4-methoxy benzyl alcohol, MeO-BnAl = 4-methoxybenzaldehyde, Me-BnOH = 4-methyl benzyl alcohol, Me-BnAl = 4-methyl benzaldehyde, BTF = trifluorotoluene, MeCN = acetonitrile, CoPz = cobalt thioporphyrazine , Ni-P = nickel bis(diphosphine)

## REFERENCES


1) Chheda, J. N.; Huber, G. W.; Dumesic, J. A. Liquid-Phase Catalytic Processing of Biomass-Derived Oxygenated Hydrocarbons to Fuels and Chemicals. *Angew. Chem. Int. Ed.* **2007**, *46*, 7164–7183.

2) Tuck, C. O.; Perez, E.; Horvath, I. T.; Sheldon, R. a.; Poliakoff, M. Valorization of Biomass : Deriving More Value from Waste. *Science* **2012**, *337*, 695–699.

3) Mika, L. T.; Cséfalvay, E.; Németh, Á. Catalytic Conversion of Carbohydrates to Initial Platform Chemicals: Chemistry and Sustainability. *Chem. Rev.* **2018**, *118*, 505–613.

4) Li, C.; Zhao, X.; Wang, A.; Huber, G. W.; Zhang, T. Catalytic Transformation of Lignin for the Production of Chemicals and Fuels. *Chem. Rev.* **2015**, *115*, 11559–11624.

5) Hu, L.; Xu, J.; Zhou, S.; He, A.; Tang, X.; Lin, L.; Xu, J.; Zhao, Y. Catalytic Advances in the Production and Application of Biomass-Derived 2,5-Dihydroxymethylfuran. *ACS Catal.* **2018**, *8*, 2959–2980.

6) Dutta, S.; De, S.; Saha, B. A Brief Summary of the Synthesis of Polyester Building-Block Chemicals and Biofuels from 5-Hydroxymethylfurfural. *ChemPlusChem* **2012**, *77*, 259–272.

7) Delidovich, I.; Hausoul, P. J. C.; Deng, L.; Pfützenreuter, R.; Rose, M.; Palkovits, R. Alternative Monomers Based on Lignocellulose and Their Use for Polymer Production. *Chem. Rev.* **2016**, *116*, 1540–1599.

8) Hu, L.; He, A.; Liu, X.; Xia, J.; Xu, J.; Zhou, S.; Xu, J. Biocatalytic Transformation of 5-Hydroxymethylfurfural into High-Value Derivatives: Recent Advances and Future Aspects. *ACS Sustain. Chem. Eng.* **2018**, *6*, 15915–15935.

9) Partenheimer, W.; Grushin, V. V. Synthesis Of 2,5-Diformylfuran and Furan-2,5-Dicarboxylic Acid by Catalytic Air-Oxidation of 5-Hydroxymethylfurfural. Unexpectedly Selective Aerobic Oxidation of Benzyl Alcohol to Benzaldehyde with Metal / Bromide Catalysts. *Adv. Synth. Catal.* **2001**, *343*, 102–111.

10) Besson, M.; Gallezot, P.; Pinel, C. Conversion of Biomass into Chemicals over Metal Catalysts. *Chem. Rev.* **2014**, *114*, 1827–1870.

11) Proctor, A. D.; Panuganti, S.; Bartlett, B. M. $CuWO_4$ as a Photocatalyst for Room Temperature Aerobic Benzylamine Oxidation. *Chem. Commun.* **2018**, *54*, 1101–1104.

12) Lang, X.; Ma, W.; Chen, C.; Ji, H.; Zhao, J. Selective Aerobic Oxidation Mediated by $TiO_2$ Photocatalysis. *Acc. Chem. Res.* **2014**, *47*, 355–363.

13) Reid, L. M.; Li, T.; Cao, Y.; Berlinguette, C. P. Organic Chemistry at Anodes and Photoanodes. *Sustain. Energy Fuels* **2018**, *2*, 1905–1927.

14) Ye, H. F.; Shi, R.; Yang, X.; Fu, W. F.; Chen, Y. P-Doped $Zn_xCd_{1-x}S$ Solid Solutions as Photocatalysts for Hydrogen Evolution from Water Splitting Coupled with Photocatalytic Oxidation of 5-Hydroxymethylfurfural. *Appl. Catal. B Environ.* **2018**, *233*, 70–79.

15) Yurdakal, S.; Palmisano, G.; Loddo, V.; Augugliaro, V.; Palmisano, L. Nanostructured Rutile $TiO_2$ for Selective Photocatalytic Oxidation of Aromatic Alcohols to Aldehydes in Water. *J. Am. Chem. Soc.* **2008**, *130*, 1568–1569.

16) Tanaka, A.; Hashimoto, K.; Kominami, H. Preparation of $Au/CeO_2$ Exhibiting Strong Surface Plasmon Resonance Effective for Selective or Chemoselective Oxidation of Alcohols to Aldehydes or Ketones in Aqueous Suspensions under Irradiation by Green Light. *J. Am. Chem. Soc.* **2012**, *134*, 14526–14533.

17) Liang, S.; Wen, L.; Lin, S.; Bi, J.; Feng, P.; Fu, X.; Wu, L. Monolayer $HNb_3O_8$ for Selective Photocatalytic Oxidation of Benzylic Alcohols with Visible Light Response. *Angew. Chemie. Int. Ed.* **2014**, *53*, 2951–2955.

18) Qamar, M.; Elsayed, R. B.; Alhooshani, K. R.; Ahmed, M. I.; Bahnemann, D. W. Highly Efficient and Selective Oxidation of Aromatic Alcohols Photocatalyzed by Nanoporous Hierarchical $Pt/Bi_2WO_6$ in Organic Solvent-Free Environment. *ACS Appl. Mater. Interfaces* **2015**, *7*, 1257–1269.

19) Kasap, H.; Caputo, C. A.; Martindale, B. C. M.; Godin, R.; Lau, V. W. H.; Lotsch, B. V.; Durrant, J. R.; Reisner, E. Solar-Driven Reduction of Aqueous Protons Coupled to Selective Alcohol Oxidation with a Carbon Nitride-Molecular Ni Catalyst System. *J. Am. Chem. Soc.* **2016**, *138*, 9183–9192.

20) Sun, X.; Luo, X.; Zhang, X.; Xie, J.; Jin, S.; Wang, H.; Zheng, X.; Wu, X.; Xie, Y. Enhanced Superoxide Generation on Defective Surfaces for Selective Photooxidation. *J. Am. Chem. Soc.* **2019**, *141*, 3797–3801.

21) Kasap, H.; Achilleos, D. S.; Huang, A.; Reisner, E. Photoreforming of Lignocellulose into $H_2$ Using Nanoengineered Carbon Nitride under Benign Conditions. *J. Am. Chem. Soc.* **2018**, *140*, 11604–11607.

22) Xu, S.; Zhou, P.; Zhang, Z.; Yang, C.; Zhang, B.; Deng, K.; Bottle, S.; Zhu, H. Selective Oxidation of 5-Hydroxymethylfurfural to 2,5-Furandicarboxylic Acid Using $O_2$ and a Photocatalyst of Co-Thioporphyrazine Bonded to g-$C_3N_4$. *J. Am. Chem. Soc.* **2017**, *139*, 14775–14782.

23) Badalyan, A.; Stahl, S. S. Cooperative Electrocatalytic Alcohol Oxidation with Electron-Proton-Transfer Mediators. *Nature.* ***2016***, *535*, 406–410.

24) Rafiee, M.; Miles, K. C.; Stahl, S. S. Electrocatalytic Alcohol Oxidation with TEMPO and Bicyclic Nitroxyl Derivatives: Driving Force Trumps Steric Effects. *J. Am. Chem. Soc.* **2015**, *137*, 14751–14757.

25) Ciriminna, R.; Palmisano, G.; Pagliaro, M. Electrodes Functionalized with the 2,2,6,6-Tetramethylpiperidinyloxy Radical for the Waste-Free Oxidation of Alcohols. *ChemCatChem* **2015**, *7*, 552–558.

26) Zhang, M.; Chen, C.; Ma, W.; Zhao, J. Visible-Light-Induced Aerobic Oxidation of Alcohols in a Coupled Photocatalytic System of Dye-Sensitized $TiO_2$ and TEMPO. *Angew. Chemie. Int. Ed.* **2008**, *47*, 9730–9733.

27) Jeena, V.; Robinson, R. S. Convenient Photooxidation of Alcohols Using Dye Sensitized Semiconductors in Combination with Silver Nitrate and TEMPO - An Electron Paramagnetic Resonance Study. *Dalt. Trans.* **2012**, *41*, 3134–3137.

28) Zhang, C.; Huang, Z.; Lu, J.; Luo, N.; Wang, F. Generation and Confinement of Long-Lived N-Oxyl Radical and Its Photocatalysis. *J. Am. Chem. Soc.* **2018**, *140*, 2032–2035.

29) Kawamata, Y.; Yan, M.; Liu, Z.; Bao, D. H.; Chen, J.; Starr, J. T.; Baran, P. S. Scalable, Electrochemical Oxidation of Unactivated C-H Bonds. *J. Am. Chem. Soc.* **2017**, *139*, 7448–7451.

30) Rafiee, M.; Wang, F.; Hruszkewycz, D. P.; Stahl, S. S. N-Hydroxyphthalimide-Mediated Electrochemical Iodination of Methylarenes and Comparison to Electron-Transfer-Initiated C-H Functionalization. *J. Am. Chem. Soc.* **2018**, *140*, 22–25.

31) Zhao, L. M.; Meng, Q. Y.; Fan, X. B.; Ye, C.; Li, X. B.; Chen, B.; Ramamurthy, V.; Tung, C. H.; Wu, L. Z. Photocatalysis with Quantum Dots and Visible Light: Selective and Efficient Oxidation of Alcohols to Carbonyl Compounds through a Radical Relay Process in Water. *Angew. Chemie. Int. Ed.* **2017**, *56*, 3020–3024.

32) Francke, R.; Little, R. D. Redox Catalysis in Organic Electrosynthesis: Basic Principles and Recent Developments. *Chem. Soc. Rev.* **2014**, *43*, 2492–2521.

33) Skubi, K. L.; Blum, T. R.; Yoon, T. P. Dual Catalysis Strategies in Photochemical Synthesis. *Chem. Rev*. **2016**, *116*, 10035–10074.

34) Yan, M.; Kawamata, Y.; Baran, P. S. Synthetic Organic Electrochemical Methods since 2000: On the Verge of a Renaissance. *Chem. Rev.* **2017**, *117*, 13230–13319.

35) Leonard, J. E.; Scholl, P. C.; Steckel, T. P.; Lentsch, S. E.; Van De Mark, M. R. Electrochemical Oxidation of Alcohols: Part II Preparative Anodic Oxidation of Secondary Alkanols Employing Lithium Nitrate. *Tetrahedron Lett*. **1980**, *21*, 4695–4698.

36) Christopher, C.; Lawrence, S.; Anbu Kulandainathan, M.; Kulangiappar, K.; Easu Raja, M.; Xavier, N.; Raja, S. Electrochemical Selective Oxidation of Aromatic Alcohols with Sodium Nitrate Mediator in Biphasic Medium at Ambient Temperature. *Tetrahedron Lett.* **2012**, *53*, 2802–2804.

37) Christopher, C.; Lawrence, S.; Bosco, A. J.; Xavier, N.; Raja, S. Selective Oxidation of Benzyl Alcohol by Two Phase Electrolysis Using Nitrate as Mediator. *Catal. Sci. Technol.* **2012**, *2*, 824–827.

38) Kroll, J. H.; Seinfeld, J. H. Chemistry of Secondary Organic Aerosol: Formation and Evolution of Low-Volatility Organics in the Atmosphere. *Atmos. Environ.* **2008**, *42*, 3593–3624.

39) Wennberg, P. O.; Bates, K. H.; Crounse, J. D.; Dodson, L. G.; McVay, R. C.; Mertens, L. A.; Nguyen, T. B.; Praske, E.; Schwantes, R. H.; Smarte, M. D.; St Clair, J. M.; Teng, A. P.; Zhang, X.; Seinfeld, J. H.. Gas-Phase Reactions of Isoprene and Its Major Oxidation Products. *Chem. Rev.* **2018**, *118*, 3337–3390.

40) Rousse, D.; George, C. A Novel Long Path Photolysis Cell - Application to the Reactivity of Selected Organic Compounds toward the Nitrate Radical ($NO_3$). *Phys. Chem. Chem. Phys.* **2004**, *6*, 3408–3414.

41) Mezyk, S. P.; Cullen, T. D.; Rickman, K. A.; Mincher, B. J. The Reactivity of the Nitrate Radical ($\bullet NO_3$) in Aqueous and Organic Solutions. *Int. J. Chem. Kinet.* **2017**, *49*, 635–642.

42) Balcerzyk, A.; El Omar, A. K.; Schmidhammer, U.; Pernot, P.; Mostafavi, M. Picosecond Pulse Radiolysis Study of Highly Concentrated Nitric Acid Solutions: Formation Mechanism of $NO_3\bullet$ Radical. *J. Phys. Chem. A* **2012**, *116*, 7302–7307.

43) Parrino, F.; Livraghi, S.; Giamello, E.; Palmisano, L. The Existence of Nitrate Radicals in Irradiated $TiO_2$ Aqueous Suspensions in the Presence of Nitrate Ions. *Angew. Chemie. Int. Ed.* **2018**, *57*, 1–6.

44) Styler, S. A.; Donaldson, D. J. Photooxidation of Atmospheric Alcohols on Laboratory Proxies for Mineral Dust. *Environ. Sci. Technol.* **2011**, *45*, 10004–10012.

45) Hering, T.; Slanina, T.; Hancock, A.; Wille, U.; König, B. Visible Light Photooxidation of Nitrate: The Dawn of a Nocturnal Radical. *Chem. Commun.* **2015**, *51*, 6568–6571.

46) Tuck, C. O.; Perez, E.; Horvath, I. T.; Sheldon, R. A.; Poliakoff, M. Valorization of Biomass: Deriving More Value from Waste. *Science* **2012**, *337*, 695–699.

47) Zhang, P.; Liu, Y.; Tian, B.; Luo, Y.; Zhang, J. Synthesis of Core-Shell Structured CdS@$CeO_2$ and CdS@$TiO_2$ Composites and Comparison of their Photocatalytic Activities for the Selective Oxidation of Benzyl Alcohol to Benzaldehyde. Catal. Today. **2017**, 281, 181-188.

48) Zhang, R.; Li, G.; Zhang, Y. Photochemical Synthesis of CdS-MIL-125(Ti) with Enhanced Visible Light Photocatalytic Performance for the Selective Oxidation of Benzyl Alcohol to Benzaldehyde. *Photochem. Photobiol. Sci.* **2017**, *16*, 996-1002.

49) Kwon, Y.; Schouten, K. J. P.; Van Der Waal, J. C.; De Jong, E.; Koper, M. T. M. Electrocatalytic Conversion of Furanic Compounds. *ACS Catal.* **2016**, *6*, 6704–6717.

50) Ibhadon, A.; Fitzpatrick, P. Heterogeneous Photocatalysis: Recent Advances and Applications. *Catalysts* ***2013***, *3*, 189–218.

51) Hudson, P. K.; Schwarz, J.; Baltrusaitis, J.; Gibson, E. R.; Grassian, V. H. A Spectroscopic Study of Atmospherically Relevant Concentrated Aqueous Nitrate Solutions. *J. Phys. Chem. A* **2007**, *111* , 544–548.

52) Boone, B. E.; Shannon, C. Optical Properties of Ultrathin Electrodeposited CdS Films Probed by Resonance Raman Spectroscopy and Photoluminescence. *J. Phys. Chem.* **1996**, *100*, 9480–9484.

53) DiMeglio, J. L.; Bartlett, B. M. The Interplay of Corrosion and Photocatalysis During Non-Aqueous Benzylamine Oxidation on Cadmium Sulfide. *Chem. Mater.* **2017**, *29,* 7579-7586

54) Wayne, R. P.; Barnes, I.; Biggs, P.; Burrows, J. P.; Canosa-Mas, C. E.; Hjorth, J.; Le Bras, G.; Moortgat, G. K.; Perner, D.; Poulet, G.; Restelli, G.; Sidebottom, H. The Nitrate Radical: Physics, Chemistry, and the Atmosphere. *Atmos. Environ. Part A, Gen. Top.* **1991**, *25*, 1–203.

55) Skov, H.; Benter, T.; Schindler, R. N.; Hjorth, J.; Restelli, G. Epoxide Formation in the Reactions of the Nitrate Radical with 2,3-Dimethyl-2-Butene, Cis- and Trans-2-Butene and Isoprene. *Atmos. Environ.* **1994**, *28*, 1583–1592.

56) Chen, B.; Wang, L.; Gao, S. Recent Advances in Aerobic Oxidation of Alcohols and Amines to Imines. *ACS Catal.* **2015**, *5*, 5851–5876.

57) Yuan, B.; Chong, R.; Zhang, B.; Li, J.; Liu, Y.; Li, C. Photocatalytic Aerobic Oxidation of Amines to Imines on $BiVO_4$ under Visible Light Irradiation. *Chem. Commun.* **2014**, *50*, 15593–15596.

58) Lang, X.; Ji, H.; Chen, C.; Ma, W.; Zhao, J. Selective Formation of Imines by Aerobic Photocatalytic Oxidation of Amines on $TiO_2$. *Angew. Chem. Int. Ed.* **2011**, *50*, 3934–3937.

59) Kwon, Y.; Schouten, K. J. P.; Van Der Waal, J. C.; De Jong, E.; Koper, M. T. M. Electrocatalytic Conversion of Furanic Compounds. *ACS Catal.* **2016**, *6*, 6704–6717.

60) Van Putten, R. J.; Van Der Waal, J. C.; De Jong, E.; Rasrendra, C. B.; Heeres, H. J.; De Vries, J. G. Hydroxymethylfurfural, a Versatile Platform Chemical Made from Renewable Resources. *Chem. Rev.* **2013**, *113*, 1499–1597.

61) Amarasekara, A. S. In Renewable Polymers. Synthesis, Processing, and Technology; Mittal, V., Ed.; Scrivener Publishing LLC: Beverly, MA, 2012; Chapter 9.

62) Zhang, N.; Zhang, Y.; Pan, X.; Yang, M. Q.; Xu, Y. J. Constructing Ternary CdS-Graphene-$TiO_2$ hybrids on the Flatland of Graphene Oxide with Enhanced Visible-Light Photoactivity for Selective Transformation. *J. Phys. Chem. C* **2012**, *116*, 18023–18031.

63) Han, G.; Jin, Y. H.; Burgess, R. A.; Dickenson, N. E.; Cao, X. M.; Sun, Y. Visible-Light-Driven Valorization of Biomass Intermediates Integrated with $H_2$ Production Catalyzed by Ultrathin Ni/CdS Nanosheets. *J. Am. Chem. Soc.* **2017**, *139*, 15584–15587.

64) Tsukamoto, D.; Ikeda, M.; Shiraishi, Y.; Hara, T.; Ichikuni, N.; Tanaka, S.; Hirai, T. Selective Photocatalytic Oxidation of Alcohols to Aldehydes in Water by $TiO_2$ Partially Coated with $WO_3$. *Chem. Eur. J.* **2011**, *17*, 9816–9824.

65) Kasap, H.; Achilleos, D. S.; Huang, A.; Reisner, E. Photoreforming of Lignocellulose into $H_2$ Using Nano-Engineered Carbon Nitride under Benign Conditions. *J. Am. Chem. Soc.* **2018**, *140*, 11604-11607.

66) Goebbert, D, J.; Garand, E.; Wende, T.; Bergmann, R.; Meijer, G.; Asmis, K. R.; Neumark, D. M. Infrared Spectroscopy of the Microhydrated Nitrate Ions $NO_3^-(H_2O)_{1\text{-}6}$. *J. Phys. Chem. A* **2009**, *113*, 7584–7592

67) Hoffmann, M. R.; Martin, S. T.; Choi, W.; Bahnemann, D. W. Environmental Applications of Semiconductor Photocatalysis. *Chem. Rev* **1995**, *95*, 69–96.

68) D. Pletcher, R. Greff, R. Peat, L. M. Peter, Instrumental Methods in Electrochemistry, Horwood, Cambridge, 2001; p. 197.

69) Lin, W. Y.; Wei, C.; Rajeshwar, K. Photocatalytic Reduction and Immobilization of Hexavalent Chromium at Titanium Dioxide in Aqueous Basic Media. *J. Electrochem. Soc.* **1993**, *140* (9), 2477–2482.

70) Zhang, M.; Wang, Q.; Chen, C.; Zang, L.; Ma, W.; Zhao, J. Oxygen Atom Transfer in the Photocatalytic Oxidation of Alcohols by $TiO_2$: Oxygen Isotope Studies. *Angew. Chemie. Int. Ed.* **2009**, *48*, 6081–6084.

71) Wang, Y.; Wang, Y.; Xu, R. Photochemical Deposition of Pt on CdS for $H_2$ Evolution from Water: Markedly Enhanced Activity by Controlling Pt Reduction Environment. *J. Phys. Chem. C* **2013**, *117*, 783–790.

TOC Graphic

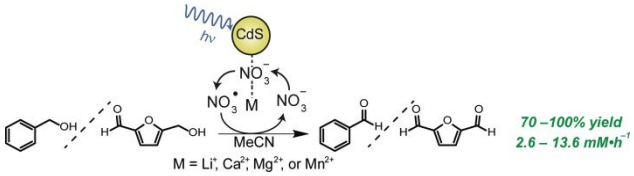
hν
CdS
NO3−
NO3• M NO3−
MeCN
M = Li+, Ca2+, Mg2+, or Mn2+
70 –100% yield
2.6 – 13.6 mM•h−1

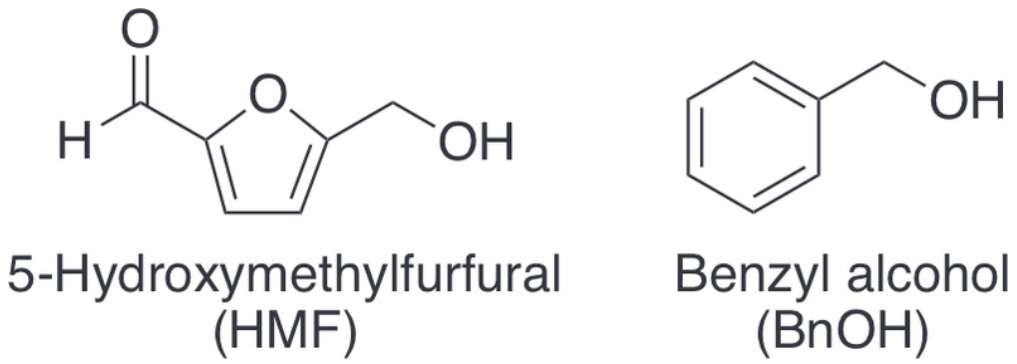


67x23mm (300 x 300 DPI)

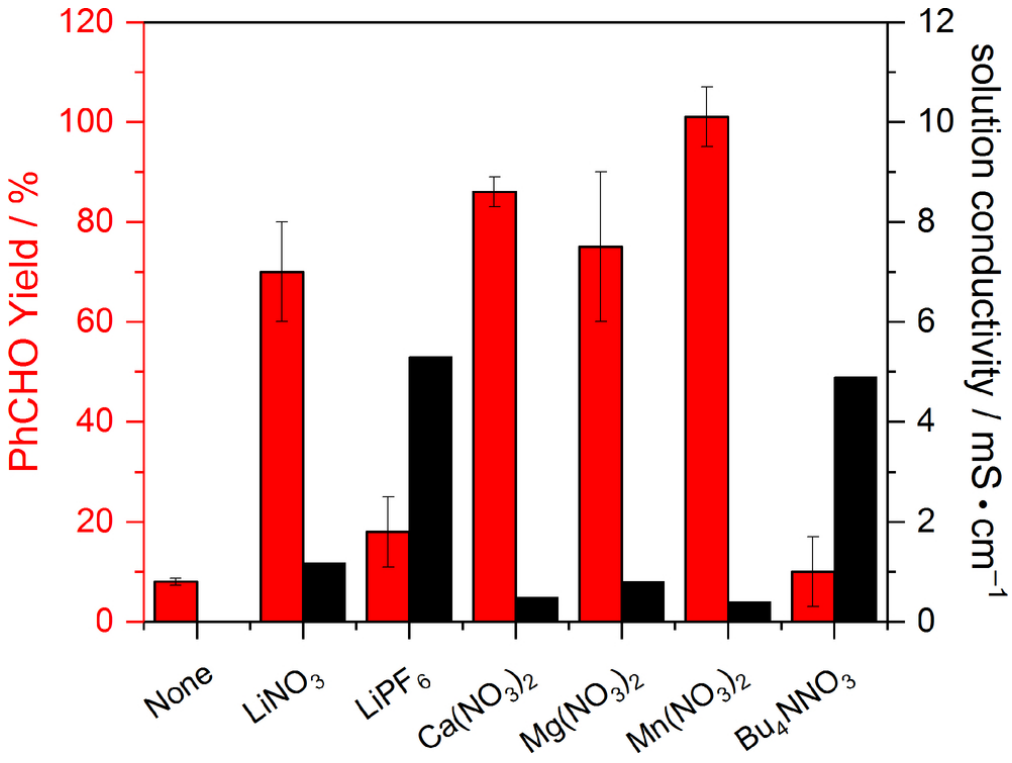


83x62mm (300 x 300 DPI)

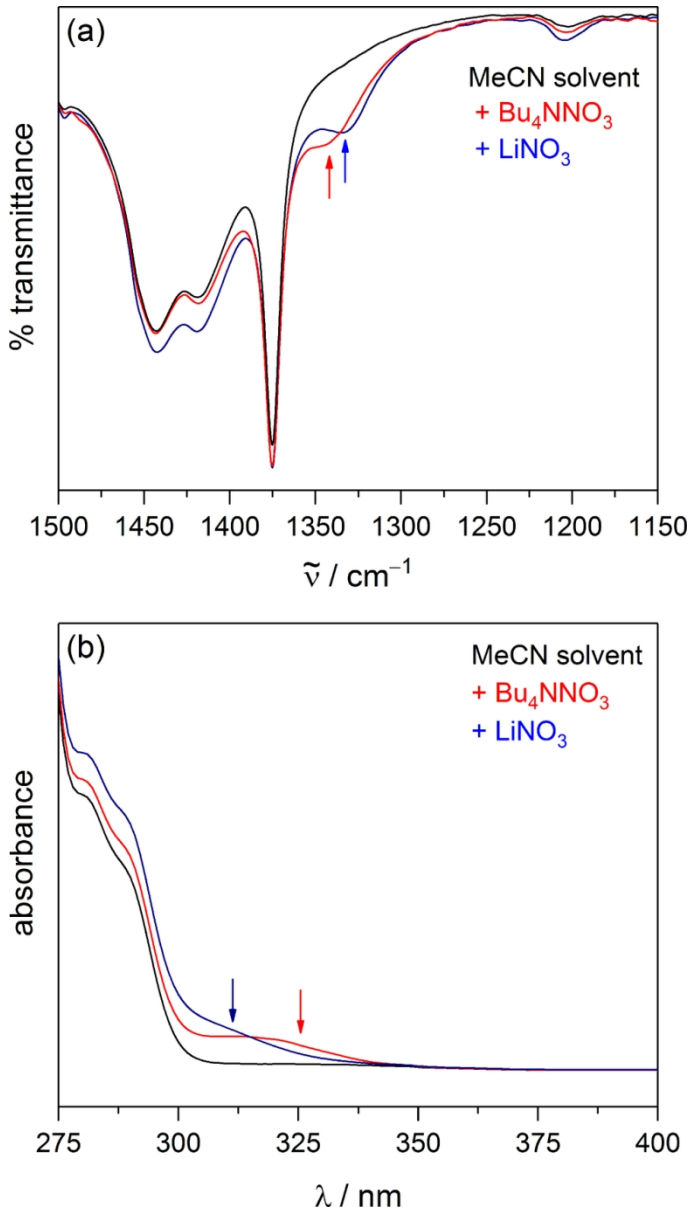


83x148mm (300 x 300 DPI)

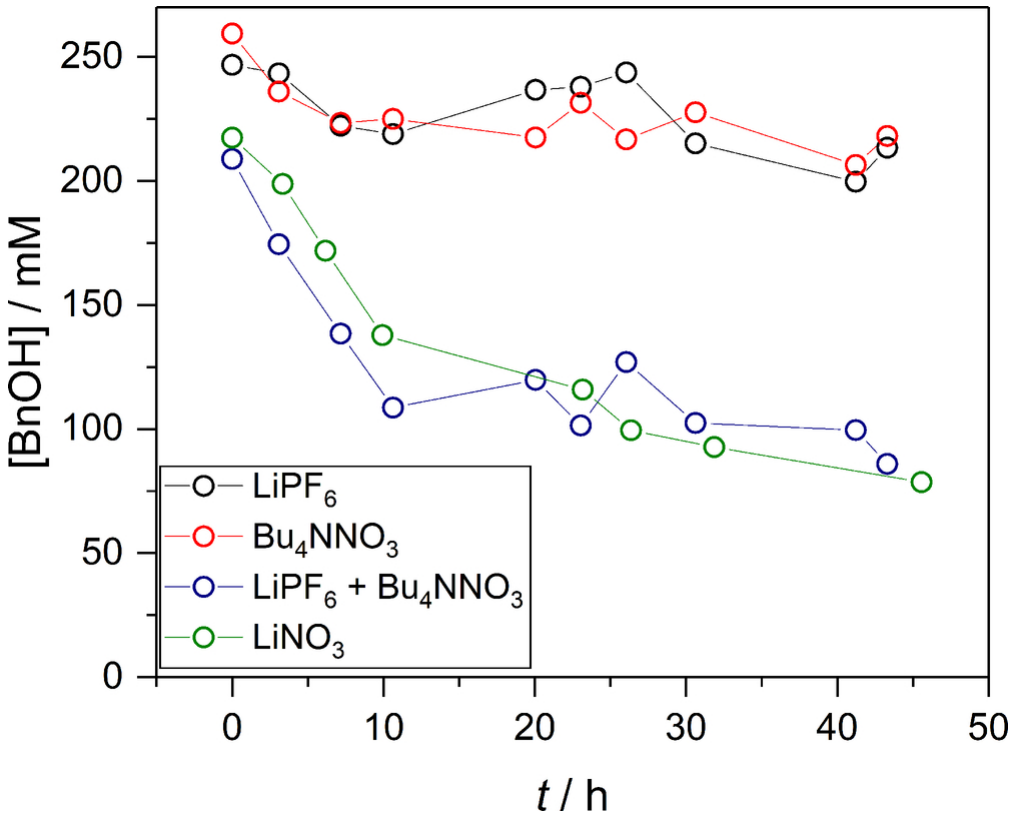


84x68mm (300 x 300 DPI)

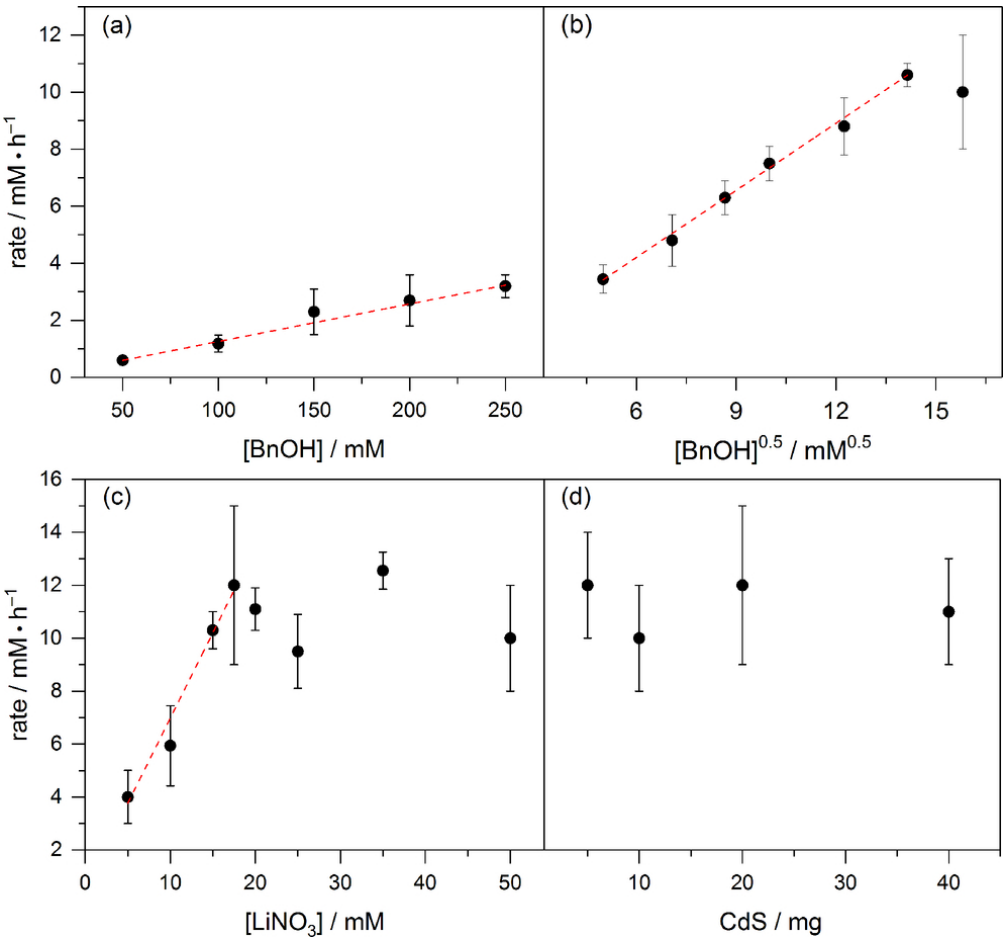


83x77mm (300 x 300 DPI)

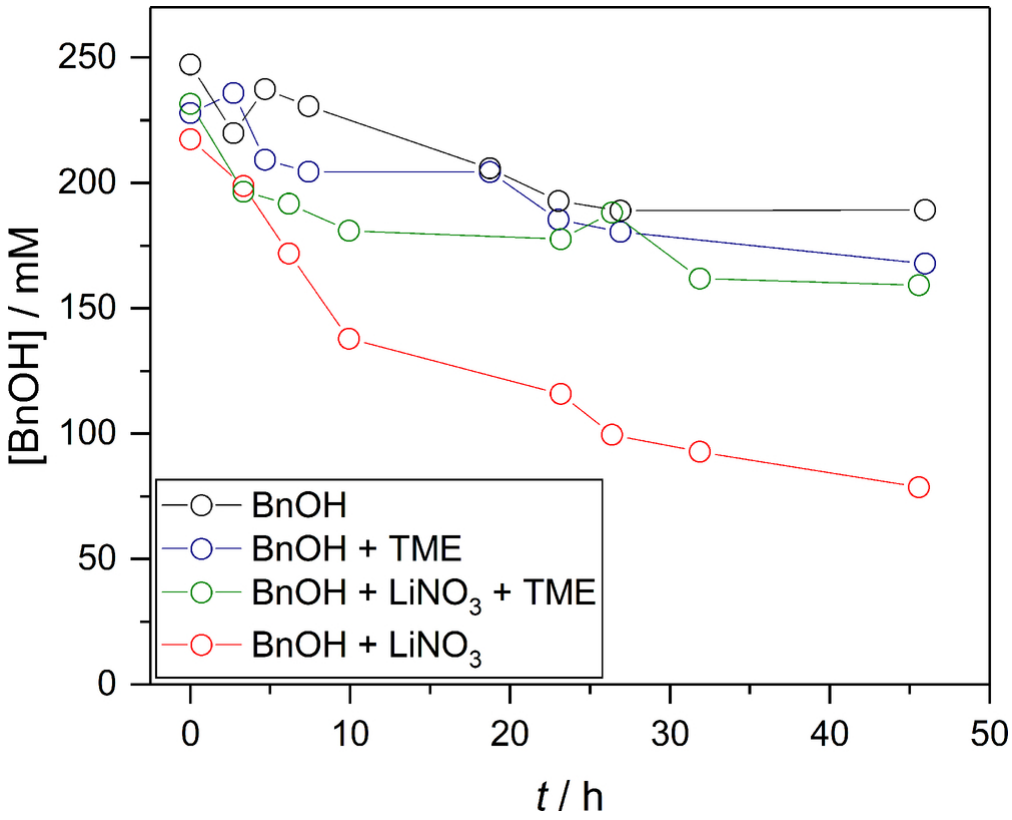


84x67mm (300 x 300 DPI)

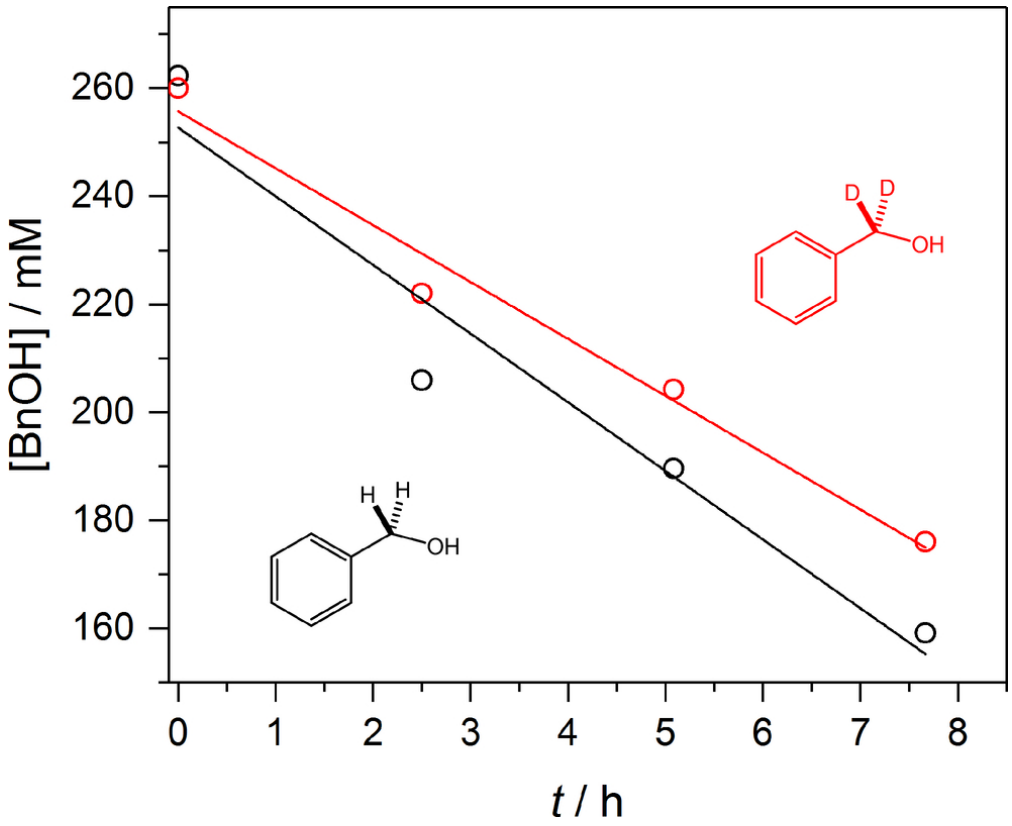


83x67mm (300 x 300 DPI)

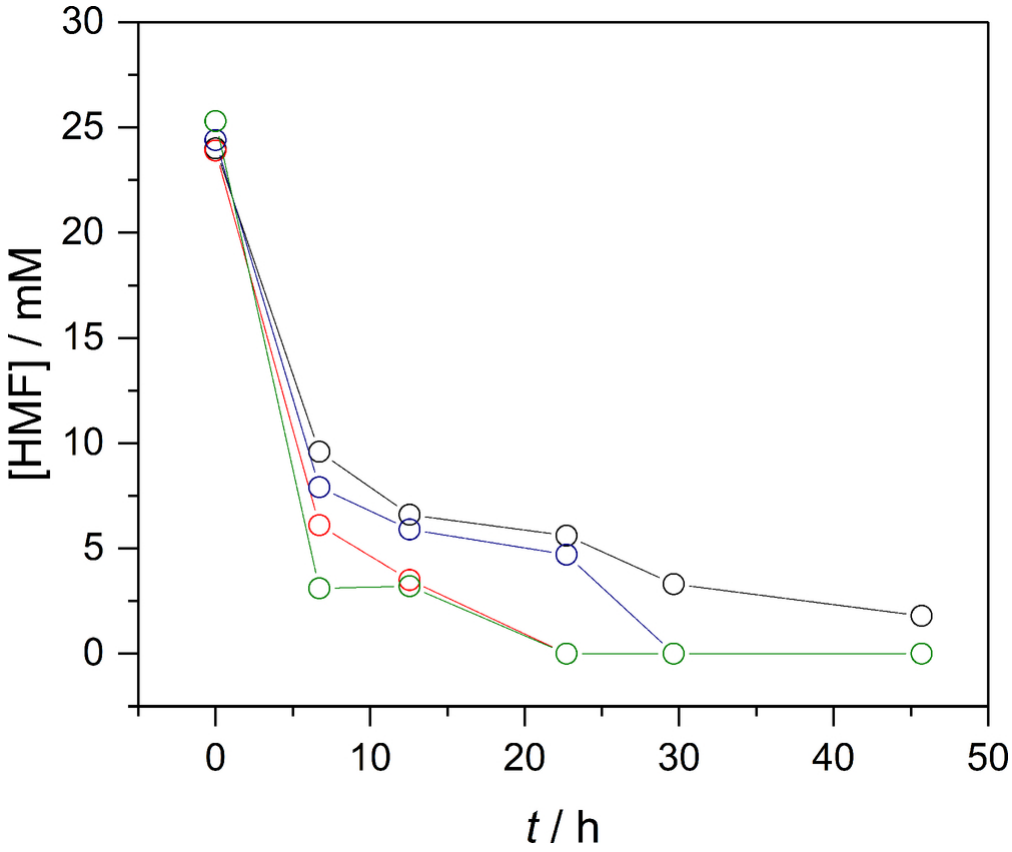


84x70mm (300 x 300 DPI)

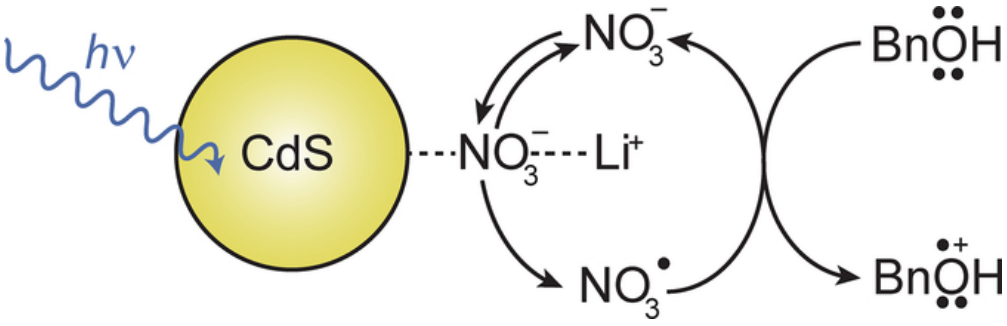


57x17mm (300 x 300 DPI)

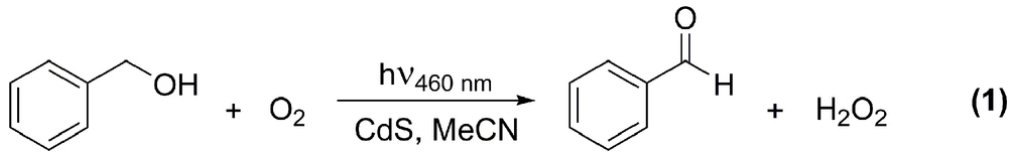


83x12mm (300 x 300 DPI)

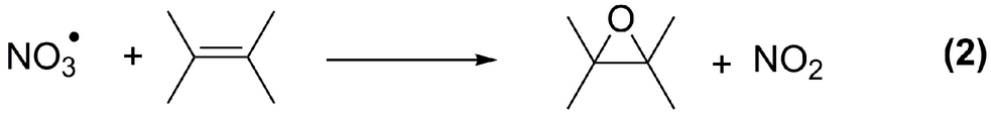


83x10mm (300 x 300 DPI)

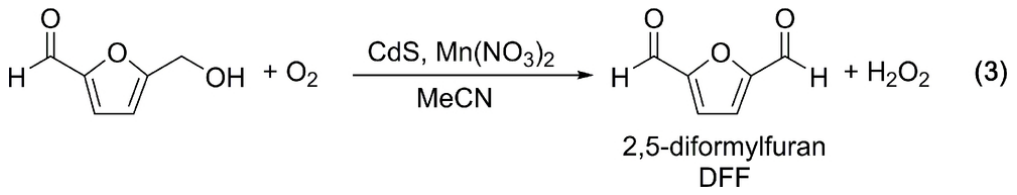


83x14mm (300 x 300 DPI)

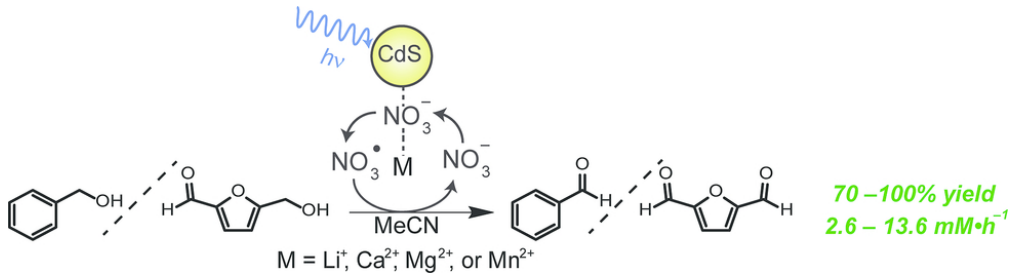


82x22mm (300 x 300 DPI)